pensations were recalculated by the HST staff and then introduced into our data analysis of each individual spectrum. This procedure and the new Doppler corrections were validated by the spectrum obtained for the sky-background measurements: The central wavelength corresponding to the Ly-α resonance line was precisely located at its laboratory value of 1215.67 Å, within the experimental accuracy (about 0.008 Å) (Fig. 1).

16. The IPM and geocoronal H also contributed some extinction to the jovian signal before it was measured by HST. The jovian profile deduced from all of these corrections was almost equal to the raw measured profile (Fig. 1). This is so because of the opposite effects of a small background subtraction and of the geocoronal and IPM extinction. Finally, we improved the measured signal-to-noise ratio by binning the spectra by pairs of pixels (for exposures of 16 min) and by four pixels (for exposures of 4 min).
17. Each mean spectrum in Fig. 2 is the average of 16 elementary exposures of $\approx$1 min. Each subspectrum in Fig. 3 is the average of four of these elementary exposures.
18. The spectral line spread function is the wavelength width measured by the instrument when exposed to an extended monochromatic source illuminating the whole detector. If a quasi-monochromatic source illuminates only one of the eight diodes of the GHRS detector, the measured width may be as small as ~0.07 Å/8 ~ 0.009 Å.
19. One such cell within the GHRS Science slit corresponds to the projection on Jupiter's disk of one GHRS diode (in the dispersion axis) by eight diodes in the perpendicular axis.
20. The bulge area can be estimated from the Voyager Ly-α isophote maps given in (4). If R_J is the jovian radius, it amounts $\pi/4 \times \pi/10 \times R_J^2 \sim 3.6 \times 10^8$ km^2.
21. C. Magnan, *Astron. Astrophys.* **144**, 186 (1985).
22. The IUE data were fitted by a total H column density [H] $\approx 3 \times 10^{17}$ to 4×10^{17} cm^{-2} [that is, three to four times the [H] derived from photochemistry models based on the Voyager Ultraviolet Spectrometer (UVS) occultation observations (9)] and velocities in the range 5 to 7 km s^{-1}. These effective velocities correspond to the active layer assumed to mimic the region where the bulge effect occurs. The integrated flux of the solar Ly-α line corresponding to the present observations was $\approx 2.6 \times 10^{11}$ photons per square centimeter per second at 1 astronomical unit.
23. The fact that these models were able to roughly fit the profiles measured by IUE appears to be due to the much longer integration time of these observations, which averaged out the fine structure of any line profile (spectral or temporal) that the higher sensitivity of HST-GHRS is now able to detect almost instantaneously.

24. The work of C.E., L.B.J., and R.P. was supported by CNRS and the Institut National des Sciences de l'Univers (INSU). The work of J.C. and G.B. was supported under NASA grant STScI GO-5417.01-93A. The work of R.G. was supported under STScI grant GO-5417.02-93A. This work is based on observations with the NASA–European Space Agency HST, obtained at the STScI, which is operated by the Association of Universities for Research in Astronomy for NASA under contract NAS 5-26535.

17 April 1996; accepted 5 July 1996

Rapid Variations in Atmospheric Methane Concentration During the Past 110,000 Years

Edward J. Brook, Todd Sowers, Joe Orchardo

A methane record from the GISP2 ice core reveals that millennial-scale variations in atmospheric methane concentration characterized much of the past 110,00 years. As previously observed in a shorter record from central Greenland, abrupt concentration shifts of about 50 to 300 parts per billion by volume were coeval with most of the interstadial warming events (better known as Dansgaard-Oeschger events) recorded in the GISP2 ice core throughout the last glacial period. The magnitude of the rapid concentration shifts varied on a longer time scale in a manner consistent with variations in Northern Hemisphere summer insolation, which suggests that insolation may have modulated the effects of interstadial climate change on the terrestrial biosphere.

Atmospheric methane concentration variations recorded in ice cores have the potential to reveal past changes in terrestrial methane emissions, driven primarily by changes in temperature and precipitation, as well as changes in the primary methane sink, oxidation by tropospheric OH. Because the atmospheric mixing time is short relative to the methane lifetime, and because methane sources and sinks have a wide geographic distribution, methane concentration variations recorded in ice cores are believed to reflect large-scale and perhaps global changes in the methane budget. Comparison of ice core methane records with other proxy climate records that are believed to reflect more regional climate variability (such as dust or the isotopic composition of ice) can provide constraints on the global significance of the regional variations.

A long record from the Vostok ice core (East Antarctica) (*1*, *2*) showed that over the past 225,000 years, atmospheric methane concentrations ranged from glacial values of ~350 parts per billion by volume (ppbV) to interglacial values of ~700 ppbV, and closely resembled patterns of summer insolation in the Northern Hemisphere (Fig. 1), which suggests that insolation variations are an important element of climate cycles controlling atmospheric methane levels (*1*, *3*). Recent work on the shallow sections of the GRIP and GISP2 ice cores from central Greenland (*4*), representing the past 40,000 years (*5*–*7*), further showed that methane concentrations varied rapidly in association with 1000- to 3000-year-long interstadial events inferred from the oxygen isotopic composition of the ice ($\delta^{18}O_{ice}$). Here we present a methane record from the GISP2 ice core for the past 110,000 years (Figs. 1 and 2). Our data verify general patterns exhibited by the Vostok methane record (*1*), verify the GRIP results between 0 and 40,000 years ago (ka) (*5*), document rapid methane variations between 40 and 110 ka, and provide a detailed picture of methane variations and their relation to interstadial events and longer term climate cycles.

We measured the methane concentration of trapped gases in samples from 309 depths in the upper 2810 m of the GISP2 ice core (*8*). Studies of ice structure (*9*), the $\delta^{18}O$ of atmospheric O_2 (*10*), and methane concentrations from the bottom 243 m of the core suggest that the stratigraphy below 2810 m is not continuous (*11*). We report the methane data (Figs. 1 and 2) on a modified GISP2 gas age time scale (*12*), which accounts for the fact that gases are trapped between 80 and 100 m below the surface of the ice sheet and are therefore younger than the surrounding ice. Within the stated uncertainties of this time scale the GISP2 methane record can be directly compared to marine and terrestrial climate records that have been placed on the calendar or SPECMAP (*12*) time scales.

The lifetime of methane in the atmosphere is relatively short, ~9 to 10 years at present (*13*, *14*). Before 1800 A.D., the dominant methane source was anaerobic decomposition of organic material in natural wetlands (*15*). Other sources including termites, wild animals, wildfires, methane hydrate release, and the oceans may have accounted for as much as 40% of total methane sources during the preindustrial Holocene and the last glacial maximum (LGM) (*15*). More recently than 1800 A.D., ice core data indicate that anthropogenic emissions significantly affected the methane cycle (*16*–*18*). The major methane sink is oxidation by tropospheric OH (*19*). Studies of the oxidative capacity of the atmosphere suggest that OH concentrations probably changed on glacial-interglacial time scales primarily in response to changing methane emissions (*20*, *21*). These results imply that the ice core methane record before 1800 A.D. primarily reflects changes in rates of emission from the dominant natural source—wetland ecosys-

E. J. Brook and J. Orchardo, Graduate School of Oceanography, University of Rhode Island, Narragansett, RI 02882, USA.
T. Sowers, 447 Deike Building, Geosciences Department, Pennsylvania State University, University Park, PA 16802, USA.

tems in the tropics and the mid-high latitude Northern Hemisphere (*1*, *5*). Similar reasoning probably also applies to the interstadial methane variations (*22*). Precipitation and temperature are the dominant factors controlling methane emissions from modern wetlands (*23*), with wetter conditions and warmer temperatures enhancing emissions. Past atmospheric methane variations therefore likely reflect changes in the hydrologic balance and temperature in methane-producing regions. Recent estimates suggest that a large fraction (40 to 70%) of total methane emissions from natural wetlands occurs in low-latitude ecosystems (*23*), which suggests that past variations in methane emissions may be, at least in part, indicative of changes in the tropical climate (*1*, *5*).

Over the 0- to 40,000-year period during which the GISP2 and GRIP records overlap, the trends and magnitudes of methane variation observed in both cores are very consistent. There are small concentration differences between the two records during the LGM (at ~20 ka), which do not affect present interpretations and are the subject of a separate intercalibration experiment (*24*). The GISP2 results verify several striking features of the Holocene methane variations (*5*, *7*), notably the high (~730 ppbV) methane concentrations during the early Holocene, the drop at ~8.2 ka to mid-Holocene values of ~575 ppbV, and the slow rise beginning at about 3 ka. The GRIP and GISP2 cores also record the dramatic methane transient during the Younger Dryas (Figs. 1 and 2A), first observed in Vostok (*1*). The event is well documented in the GISP2 core by a 150-ppbV drop in atmospheric methane levels at about 13 ka, followed by low values of ~460 to 525 ppbV for the next ~1000 years and a well-defined rapid increase to ~730 ppbV at 11.7 ka (Figs. 1 and 2). Nine samples from depths between 1695 and 1702 m define the latter transition, during which atmospheric methane levels increased by ~220 ppbV in ~260 years. This rate of increase (~0.9 ppbV/year) is similar to the rate of increase in the early 1800s, which was largely the result of increased anthropogenic emissions. Within the estimated uncertainty in the ice age–gas age difference of ±350 years (*12*), the methane and isotopic temperature changes at the end of the Younger Dryas are in phase. This conclusion is consistent with preliminary results of a more precise technique of examining ice age–gas age differences, which takes advantage of the preservation of an isotopic signal caused by thermal fractionation of nitrogen isotopes in firn air at times of rapid surface temperature change (*25*).

In contrast, the initial methane increase near the end of the last glacial period (Fig. 2A) occurred at 17 ka (GISP2 chronology), which is before the major isotopic temperature increase associated with the transition from the Oldest Dryas to the Bølling period (14.7 ka in the GISP2 chronology) but is coincident with the deglacial temperature increase observed in the Byrd (Antarctica) ice core (*26*). Methane levels increased in two distinct steps between 17 and 14.7 ka (Fig. 2A). The first, at 17 ka, was followed by 1000 years of reduced growth (and perhaps even a slight reversal in the GRIP record) between 16 and 15 ka. This event coincides with the last Heinrich event, during which iceberg discharge from the Laurentide, Scandinavian, and Icelandic ice sheets cooled the north Atlantic region (*27*). Methane levels next increased at the onset of the Bølling period (Figs. 1 and 2A). These observations suggest that the deglacial methane increase was initiated by climate change outside of the high-latitude Northern Hemisphere (that is, in the tropics); was subsequently slowed, perhaps by cooling caused by the Heinrich event; and was then accelerated by the rapid climate shift at the beginning of the Bølling period.

The earlier part of the GISP2 methane record (20 to 110 ka; Fig. 1) is consistent with the general pattern documented in the Vostok record (*1*), exhibits all the high-frequency methane variations documented in the GRIP methane record between 20 and 40 ka (*5*), and demonstrates that these high-frequency variations occurred throughout the last glacial period. The detailed record during marine isotope stage 3 (MIS-3) (22 to 60 ka; Fig. 2B) demonstrates that the maximum methane concentration reached during interstadial events varied. The highest concentrations during this interval occurred at ~58, ~45, and ~38 ka (interstadials 16/17, 12, and 8, respectively). After each of these elevated methane events, concentrations gradually declined over the following 7000 to 20,000 years. This pattern is qualitatively similar to the long-term cooling cycles identified in North Atlantic proxy temperature records (*27*). These long-term cooling cycles began with an abrupt warming episode that generally followed a Heinrich event (*27*) (Fig. 1). Our data suggest that climate changes associated with this warming, and the subsequent cooling, may have affected the terrestrial environments responsible for methane production.

Although rapid changes in methane concentration are prevalent throughout our record, the transition between MIS-4 and

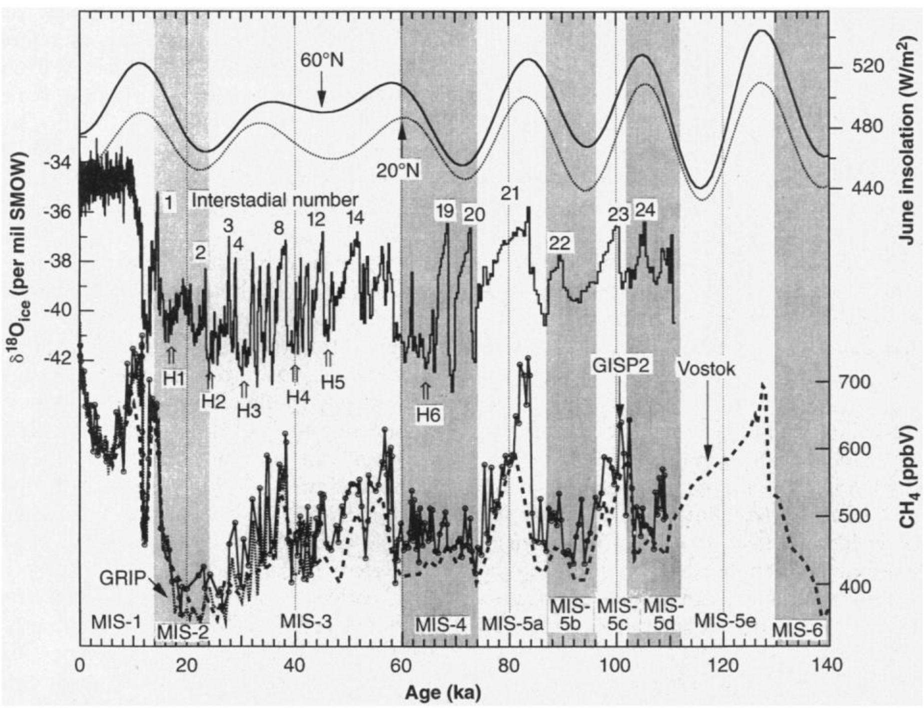

Fig. 1. Comparison on a common time scale (*12*) of GISP2 (lower solid line), GRIP (lower dotted line) (*5*, *7*), and Vostok (lower heavy dashed line) (*1*) methane records with Northern Hemisphere June insolation at 60°N (upper solid line) and 20°N (upper dotted line) (*36*) and the GISP2 $\delta^{18}O_{ice}$ record (*37*). We plotted both insolation curves to illustrate the previously noted similarities between the atmospheric methane history and both low- (*1*) and high-latitude (*34*) climate change. MIS boundaries are taken from (*38*). The plotted GISP2 points are average values for each depth. Individual replicates are plotted in Fig. 2. Heinrich events (H1 through H6) are placed relative to the ice core $\delta^{18}O_{ice}$ record based on previously proposed correlations of marine and Greenland ice core records (*28*).

MIS-3 (58 ka) marks a distinct change in the character of the variations. During the ~15,000-year period immediately preceding the MIS-4/MIS-3 transition, methane levels were relatively stable and low (between 400 and 500 ppbV), with maximum fluctuations of ~50 ppbV, despite the two large interstadial events (interstadials 19 and 20) that occurred early in MIS-4 (Fig. 2C). These events, which occurred during a minimum in Northern Hemisphere insolation, lasted ~2000 years. The resolution of the GISP2 methane record in this interval is on average ~500 years, so it is unlikely that our record missed larger fluctuations. The observation of minimal methane variation during these two interstadial events supports the contention that methane variations did not contribute to the large temperature oscillations associated with other interstadial events (*5*). Also, if methane levels are intimately tied to the tropical hydrologic cycle as previously proposed (*1*, *5*), this observation poses a difficulty for hypotheses that suggest that variations in the water vapor content of the atmosphere might drive interstadial warming. Why did methane levels remain low during these events? Aridity in the tropics, which has been linked to the insolation minimum at this time (*28*, *29*) may be important. Another potentially important factor is that the substantial increase in continental ice volume during the MIS-5/MIS-4 transition (*30*) may have covered boreal areas that today produce substantial quantities of methane (*5*, *19*, *31*) and reduced potential response to interstadial warming. Methane concentrations were also low during times of reduced Northern Hemisphere summer insolation (and ice volume) at ~ 25, ~45, and ~95 ka despite substantial variations in isotropic temperature (Fig. 1).

In contrast, large methane peaks are associated with MIS-5a and MIS-5c (at ~84 and 102 ka). The maximum methane values recorded in the GISP2 core in MIS-5a exceed 700 ppbV. Such high methane levels are only observed during the Holocene and Bølling periods in the GISP2 record (Figs. 1 and 2). The $\delta^{18}O_{ice}$ values for MIS-5a are, however, slightly lower (indicating cooler temperatures) than for the Bølling period or the Holocene. In addition, the abrupt methane increase at the onset of MIS-5a is coincident with the rapid temperature increase at the beginning of interstadial 21. During MIS-5c there are two distinct peaks in the GISP2 record, which are features not previously observed in the lower resolution Vostok record. The initial increase in methane concentration (at the end of MIS-5d) is coeval with an increase in the Vostok record (Fig. 1) but appears to lead the temperature increase at interstadial 23 by as much as 2000 years. A lead of this magnitude is unlikely to be related to errors in our ice age–gas age calculations during this period (estimated uncertainty is ~350 years). However, we cannot completely exclude systematic errors in the gas age time scale or subtle stratigraphic disturbances as the cause of the apparent lead. If our record is correct, however, it suggests a decoupling of Greenland temperatures and methane emissions during this time period, as is also observed in the Holocene (*7*). Furthermore, the rapid methane oscillation at ~101 ka is not clearly related to any similar feature in the GISP2 $\delta^{18}O_{ice}$ record but does appear to correlate with features in some other proxy records. For example, Keigwin *et al.* (*32*) noted a similar oscillation at about the same time in proxy records of North Atlantic thermohaline circulation. They also correlated this event with the "Montaigu period," a brief stadial event observed in some long European pollen records (*33*).

With the exception of the event during MIS-5c, the increases in methane concentration at the beginning of the interstadial events are in phase, within the 350-year uncertainty in the ice age–gas age difference (*12*), with the coeval events in the $\delta^{18}O_{ice}$ records, which supports the hypothesis that they have a common origin. As mentioned previously, ecosystem-level studies show that methane production in wetlands is enhanced by increased temperature and precipitation, although other factors also play important roles (*19*, *31*). The interstadial methane peaks therefore represent the direct response of methane production to increased temperatures, a response to associated changes in the hydrologic cycle (*5*), or some combination of the two.

The GISP2 data also reveal the nature of methane variations within Dansgaard-Oeschger cycles. Data from interstadial events 8, 12, 14, and 21 (Fig. 2) show that methane concentration variations were closely tied to the $\delta^{18}O_{ice}$ record. Concentrations rose rapidly at the beginning of each event and then fell gradually, following the trend of isotopic temperature (Fig.

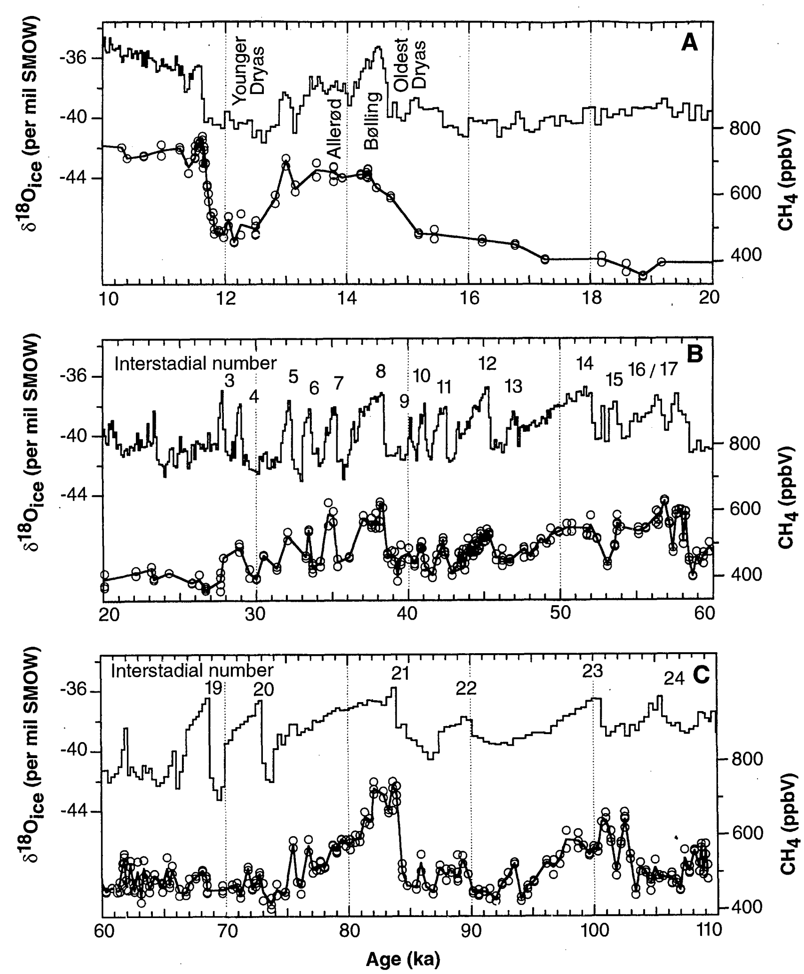

Fig. 2. Expanded plots of the GISP2 methane and $\delta^{18}O_{ice}$ records (Fig. 1). (**A**) Data from 10 to 20 ka; (**B**) data from 20 to 60 ka; and (**C**) data from 60 to 110 ka. All replicate methane measurements are shown as circles, and the solid line connecting them passes through the mean value for each depth. Thin solid line in upper half of each panel is $\delta^{18}O_{ice}$ record from (*37*).

2). In the best-resolved case, interstadial 8, the increase in methane levels at the beginning of the event (an ~150 ppbV change in ~100 years) rivals the rapidity of the increase at the end of the Younger Dryas. The close correspondence between the trends in methane and temperature at the beginning of and during the interstadial events provides further evidence for a tight link between the interstadial events observed in Greenland and the methane budget. It is also interesting to note that, throughout the last glacial period, methane concentrations during intervening stadial (cold) periods were consistently ~450 ppbV, regardless of the overall state of the climate system (in regard to insolation or ice volume, for instance). This observation may indicate that a baseline level of methane production near, but slightly higher than, full glacial levels was maintained by a mechanism (perhaps methane production in tropical wetlands) that was relatively insensitive to longer term climatic change. The abrupt warming episodes (or their underlying causal mechanism) that mark the beginning of interstadial events appear to have triggered large changes in the methane budget.

The rapidity and magnitude of the methane shifts argue for large-scale regional-to-global changes in terrestrial climate associated with interstadial events. For example, the large methane changes (up to ~300 ppbV at interstadial 21) during many of the interstadial events imply a change in methane source strength of up to ~50 Tg of CH_4 per year [using calculations in (*15*)]. This value is about 50% of total emissions from wetlands today (*19, 31*). It is unlikely that the North Atlantic region, where much of the evidence for rapid climate change associated with the interstadial events has been gathered (*27*), could have alone supported such a large emission rate change during the glacial period. Based on the GRIP record, Chappellaz *et al.* (*5*) hypothesized that methane production in tropical wetlands was increased substantially as a result of interstadial climate shifts. However, it has also been suggested that high-latitude wetlands in ice-free areas might have been important methane sources during the glacial period (*1, 15, 34*). We speculate that rapid warming during interstadial events, particularly during MIS-3 when other evidence suggests substantial reductions in ice volume (*35*), might have triggered increases in methane emissions from high-latitude wetlands in addition to influencing tropical emissions. Future studies to determine the interpolar methane gradient and the isotopic composition of atmospheric methane during these events may shed light on this issue.

Finally, the GISP2 methane record reveals that the atmospheric methane concentration varied on two time scales in the past 110,000 years. Rapid variations occurred on interstadial time scales, but these variations were apparently modulated on a longer time scale in a manner consistent with orbital forcing (Fig. 1). Our results suggest that the broad methane peaks in the low-resolution Vostok record (*1*) are actually groups of methane maxima and that each peak appears to be related to an interstadial event. The amplitude of the methane variations during interstadials varied, reaching maximum values during Northern Hemisphere summer insolation maxima during the last 110,000 years and minimum values during insolation minima. Variations in Northern Hemisphere summer insolation caused by the Earth's orbital precession cycle, which has 19,000- and 23,000-year periodicities, were previously linked (*1*) to variations of the tropical monsoon cycle (*29*) and to methane emissions in the tropics. Summer insolation variations at high latitudes exhibit similar periodicities (Fig. 1), which may also have affected past methane budgets, perhaps through the combined effects on the growth and decay of Northern Hemisphere ice sheets (and therefore high-latitude wetland area) and through direct effects on the hydrology and temperature of wetlands in ice-free regions of the high-latitude Northern Hemisphere (*34*). Both factors may have been important, but our results suggest that climate variations on oribital time scales were not directly related to past variability in atmospheric methane. Instead, the longer term climate cycles appear to have modulated the amplitude of the methane response to millennial-scale climate change.

REFERENCES AND NOTES

1. J. Chappellaz, J. M. Baranola, D. Raynaud, Y. S. Korotkevich, C. Lorius, *Nature* **345**, 127 (1990).
2. J. Jouzel *et al.*, *ibid.* **364**, 407 (1993).
3. Spectral analysis of the Vostok methane record showed significant power in the 122,000-, 42,000-, 25,000-, and 19,000-year spectral bands, which is similar to Earth's orbital frequencies of eccentricity, obliquity, and precession (*1, 2*). This finding suggests that the atmospheric methane cycle is strongly influenced by variations in the seasonality and latitudinal distribution of incident solar insolation.
4. The GRIP and GISP2 ice cores were drilled to bedrock in central Greenland (GISP2: 72°36'N, 38°30'W; GRIP: 72°18' N, 37°37'W) about 28 km apart.
5. J. Chappellaz et *al.*, *Nature* **366**, 443 (1993).
6. M. Bender, T. Sowers, J. Orchardo, *Eos* **74(43)**, 78 (1993).
7. T. Blunier, J. Chappellaz, J. Schwander, B. Stauffer, D. Raynaud, *Nature* **374**, 46 (1995).
8. Ice samples weighing ~35 g were placed in a stainless steel vacuum vessel designed to reduce dead volume. Samples were maintained at −20°C and ambient air was pumped out with a vacuum pump. Samples were melted in vacuo, then refrozen slowly at −100°C to transfer the gas to the head space above the ice. The gas was directly expanded into an evacuated 10-cm^3 sample loop and injected onto a Poropak Q column in an HP 5890 Series II gas chromatograph. Methane was detected with a flame ionization detector. Sample concentrations were quantified with the use of air standards that were calibrated to the National Oceanic and Atmospheric Association/Climate Monitoring and Diagnostics Laboratory (NOAA/CMDL) methane scale. Our working standard was 962 ± 6 ppbV (95% confidence interval). Sample concentrations were reproducible to ±2% of the mean of replicate analyses. The blank was quantified by addition of standard gas to a vessel containing a previously degassed ice sample and analysis of that gas after melting and refreezing the ice. Blank corrections were 15 ± 8 ppbV (95% confidence interval, n = 42) after September 1993 and 8 ± 15 ppbV (95% confidence interval, n = 7) before September 1993. The data will be available from the NOAA World Data Center–A by anonymous FTP at ftp.ngdc.noaa.gov or on the World Wide Web at http://www.ngdc.noaa.gov/paleo/paleo.html.
9. R. B. Alley *et al.*, *Nature* **373**, 393 (1995)
10. M. Bender *et al.*, *ibid.*, p. 663.
11. E. Brook, M. Bender, J. Orchardo, T. Sowers, *Eos* **74**, 381 (1994); J. Chappellaz, E. Brook, T. Blunier, B. Malaize, in preparation.
12. The GISP2 time scale was derived by counting of annual layers in the core back to 50 ka [D. Meese *et al.*, *Special Report 94-1* (Cold Regions Research and Engineering Lab, Hanover, NH (1994); R. Alley *et al.*, *Nature* **362**, 527 (1993)]. Before 50 ka, the dating was derived by correlation of the $\delta^{18}O$ of atmospheric O_2 records from GISP2 into the Vostok record (*10*) and correcting for ice age–gas age differences as described below. Uncertainties in the absolute ice age time scale for GISP2 are 1% between 0 and 11.7 ka, 5% between 11.7 and 55 ka, and less than 3000 years between 55 and 110 ka. Estimates of the ice age–gas age differences (Δage) were made as in T. Sowers, M. Bender, D. Raynaud, Y. S. Korotkevich, *J. Geophys. Res.* **97**, 15683 (1992). Two estimates of the paleo-surface temperature were made with the use of different $\delta^{18}O_{ice}$/temperature calibration factors {α = 0.67 and 0.33 per mil per degree Celsius [K. Cuffey *et al.*, *Science* **270**, 455 (1995)]}. These Δage estimates define a plausible range for this parameter. For the coldest periods of the last glacial period, the two Δage values differ by as much as 700 years, depending on the α value used. We averaged the two Δage estimates all along the core to construct the gas age–depth relation for GISP2, which is used to plot methane data in Figs. 1 and 2. We consider the uncertainty in our Δage estimates to be ±100 years after 10 ka and ±350 before 10 ka. Because the existing time scale for GRIP does not exactly agree with the GISP2 time scale, for Fig. 1 we mapped the GRIP $\delta^{18}O_{ice}$ record into the GISP2 $\delta^{18}O_{ice}$ record and applied our Δage estimates from the GISP2 core to the modified GRIP time scale, following T. Sowers, M. Bender, D. Raynaud, Y. S. Korotkevich, *J. Geophys. Res.* **97**, 15683 (1992). The Vostok time scale in Fig. 1 is based on correlation with the SPECMAP (spectral mapping project) time scale and is from T. Sowers *et al.* [*Paleoceanography* **8**, 737 (1993)].
13. R. Prinn *et al.*, *Science* **238**, 945 (1987).
14. R. G. Prinn *et al.*, *ibid.* **269**, 187 (1995).
15. J. Chappellaz, I. Y. Fung, A. M. Thompson, *Tellus* **45B**, 228 (1993).
16. H. Craig and C. C. Chou, *Geophys. Res. Lett.* **9**, 1221 (1982); R. A. Rasmussen and M. A. K. Khalil, *J. Geophys. Res.* **89**, 11599 (1984).
17. T. Blunier *et al.*, *Geophys. Res. Lett.* **20**, 2219 (1993).
18. D. M. Etheridge, G. I. Pearman, P. J. Fraser, *Tellus* **44B**, 282 (1992).
19. D. H. Ehhalt, *ibid.* **26**, 58 (1972).
20. A. M. Thompson, *Science* **256**, 1157 (1992); ______, J. A. Chappellaz, I. Y. Fung, T. L. Kucsera, *Tellus* **45B**, 242 (1993).
21. P. Martinerie, G. P. Brasseur, C. Granier, *J. Geophys. Res.* **100**, 14, 291 (1995).
22. As previously discussed for glacial-interglacial

warming, increasing temperatures would probably lead to increases in OH formation rates (*20*, *21*) and an increase in the reaction rate between methane and OH [D. Raynaud, J. Chappellaz, J. M. Baranola, Y. S. Korotkevich, C. Lorius, *Nature* **333**, 655 (1988)], and therefore to increased rates of methane destruction. If so, the association of interstadial events with increased methane concentration suggests that methane source strength probably did not decrease and may have increased to a greater extent than indicated by the concentration variations.
23. I. Fung *et al.*, *J. Geophys. Res.* **96**, 13033 (1991); K. Bartlett and R. Harris, *Chemosphere* **26**, 26 (1993).
24. Measurements of standard gas samples have routinely been exchanged between various labs measuring methane in ice cores. The concentration scales in the Laboratoire de Glaciologie in Grenoble and at the Physics Institute at the University of Bern appear to be 2.0% and 1.0% higher, respectively, than the NOAA/CMDL methane scale (T. Sowers *et al.*, in preparation). The GRIP concentrations were therefore lowered by 2% relative to the GISP2 data.
25. J. Severinghaus and T. Sowers, *Eos* **76**, F291 (1995); J. Severinghaus, E. Brook, T. Sowers, R. Alley, *ibid.* **77**, S157 (1996).
26. T. Sowers and M. Bender, *Science* **269**, 210 (1995).
27. G. Bond *et al.*, *Nature* **360**, 245 (1992); G. Bond *et al.*, *ibid.* **365**, 143 (1993).
28. N. Petit-Maire, M. Fontugne, C. Rouland, *Palaeogeogr. Palaeoclimatol. Palaeoecol.* **86**, 197 (1991).
29. W. L. Prell and J. E. Kutzbach, *J. Geophys. Res.* **92**, 8411 (1987).
30. N. J. Shackleton, *Quat. Sci. Rev.* **6**, 183 (1987); A. C. Mix, *Geol. Soc. Am. Spec. Pap.* **270**, 19 (1992).
31. E. Matthews, in *Atmospheric Methane: Sources, Sinks, and Global Change*, M. A. K. Khalil, Ed. (Springer-Verlag, New York, 1993), pp. 314–361.
32. L. Keigwin, W. B. Curry, S. J. Lehman, S. Johnsen, *Nature* **371**, 323 (1994).
33. D. P. Adam, J. D. Sims, C. K. Throckmorton, *Geology* **9**, 373 (1981); G. Woillard, *Quat. Res.* **9**, 1 (1978); P. C. Tzedakis, *Nature* **364**, 437 (1993).
34. T. Crowley, *Nature* **353**, 122 (1991).
35. N. J. Shackleton, *Quat. Sci. Rev.* **6**, 183 (1987).
36. A. Berger and M. F. Loutre, *ibid.* **10**, 297 (1991).
37. P. Grootes, M. Stuiver, J. W. C. White, S. Johnsen, J. Jouzel, *Nature* **366**, 552 (1993); M. Stuiver, P. Grootes, T. Braziunas, *Quat. Res.* **44**, 341 (1995).
38. D. G. Martinson *et al.*, *Quat. Res.* **27**, 1 (1987).
39. Supported by grants from NSF. E.J.B was also supported by a NOAA Climate and Global Change postdoctoral fellowship. We thank M. Bender and R. Alley for comments on the manuscript and M. Swanson for laboratory assistance.

22 March 1996; accepted 2 July 1996

Late Pleistocene Desiccation of Lake Victoria and Rapid Evolution of Cichlid Fishes

Thomas C. Johnson,* Christopher A. Scholz, Michael R. Talbot, Kerry Kelts, R. D. Ricketts, Gideon Ngobi, Kristina Beuning, Immacculate Ssemmanda, J. W. McGill

Lake Victoria is the largest lake in Africa and harbors more than 300 endemic species of haplochromine cichlid fish. Seismic reflection profiles and piston cores show that the lake not only was at a low stand but dried up completely during the Late Pleistocene, before 12,400 carbon-14 years before the present. These results imply that the rate of speciation of cichlid fish in this tropical lake has been extremely rapid.

Lake Victoria is second only to Lake Malawi in diversity of endemic species of cichlid fish (*1*). This rich diversity is somewhat surprising because Lake Victoria is known to be relatively young as compared with the large lakes occupying the East African Rift Valley. The rich diversity in Lake Victoria implies that its cichlid species flock evolved rapidly. But how rapidly? Did most of the species evolve over a span of a few hundred thousand years since the lake first formed, or did they appear more recently, since the lake was at a low stand during the late Pleistocene, when much of north and equatorial Africa was dry (*2*, *3*)? Were there small satellite lakes in the Victoria basin where these hundreds of species of cichlids could seek refuge and wait out the late Pleistocene arid period? If not, the rate of evolution of Lake Victoria's cichlids is the fastest ever recorded for such a large number of vertebrate species.

T. C. Johnson and R. D. Ricketts, Large Lakes Observatory, University of Minnesota, Duluth, MN 55812, USA.
C. A. Scholz, Rosenstiel School of Marine and Atmospheric Sciences, University of Miami, Miami, FL 33149, USA.
M. R. Talbot, Geological Institute, University of Bergen, 5007 Bergen, Norway.
K. Kelts, G. Ngobi, K. Beuning, Limnological Research Center, University of Minnesota, Minneapolis, MN 55455, USA.
I. Ssemmanda, Department of Geology, Makerere University, Post Office Box 7062, Kampala, Uganda.
J. W. McGill, Embangweni Hospital, Post Office Box 7, Embangweni, Malawi.

*To whom correspondence should be addressed.

We surveyed the floor of Lake Victoria in March and April 1995, using seismic reflection profiling and piston coring as part of the first expedition of the International Decade for the East African Lakes (IDEAL). One of the major objectives was to determine how much smaller Lake Victoria was during the late Pleistocene than today.

Lake Victoria straddles an ancient drainage system that flowed from east to west and was modified by uplift on the shoulder of the Albert Rift (*4*). Although this tectonic activity may have begun in the Miocene, river downcutting maintained westward drainage until the Pleistocene, when flow reversal created a lake substantially larger than the present one (*5*). Precisely when this occurred in the Pleistocene is not known. Doornkamp and Temple (*5*) and Bishop and Posnansky (*6*) estimated a middle to late Pleistocene age for the lake of [younger than 0.8 million years ago (Ma)] on the basis of lacustrine sequences exposed in the Kagera River valley approximately 100 km west of the lake and 130 m above its present surface. Kent (*7*) estimated an early to middle Pleistocene age (1.6 to 0.8 Ma), on the basis of lacustrine sequences 100 m above the present lake near the Kavirondo Gulf on the Kenyan side of the lake.

The lake level has varied by about 2 m during the past century in response to variations in rainfall and evaporation (*8*), and the lake was at least 65 m lower than at present at the end of the last glaciation, between 15,000 and 17,000 years before present (B.P.) (*9*). Lake Victoria's maximum depth is only 69 m, so the issue of whether one or more residual lakes survived this late Pleistocene arid interval, providing refuges for the extraordinary species richness of the lake's cichlid faunas, has been debated (*1*–*3*).

In our survey, we used an intermediate-resolution seismic reflection profiling system (Fig. 1) (*10*). Reconnaissance seismic profiles had been obtained along four track lines across Lake Victoria in the late 1980s

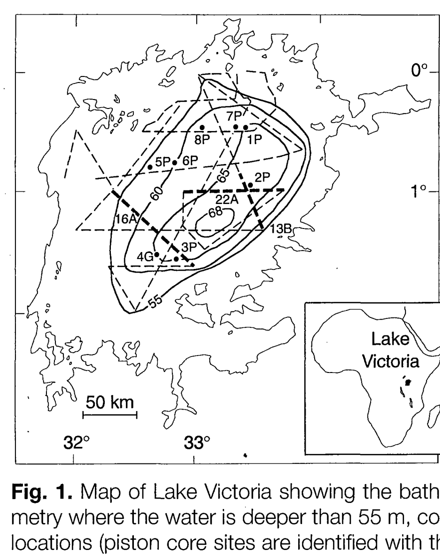

Fig. 1. Map of Lake Victoria showing the bathymetry where the water is deeper than 55 m, core locations (piston core sites are identified with the suffix P and the gravity core site with the suffix G), and seismic survey track lines (light dashed lines). Water depths are in meters (we have assumed a speed of sound of 1500 m/s). Locations of seismic reflection profiles in Fig. 3 are depicted with heavy dashed lines.